STEM CELLS AND DEVELOPMENT
Volume 32, Numbers 19–20, 2023

DOI: 10.1089/scd.2023.0038

Fate Specification of GFAP-Negative Primitive Neural Stem Cells and Their Progeny at Clonal Resolution

Samantha Z. Yammine,[1] Ian Burns,[1] Jessica Gosio,[1,2] Andrew Peluso,[1] Daniel M. Merritt,[3] Brendan Innes,[1] Brenda L.K. Coles,[1] Wen Rui Yan,[1] Gary D. Bader,[1,4] Cindi M. Morshead,[4,5] and Derek van der Kooy[1,4]

The mature brain contains an incredible number and diversity of cells that are produced and maintained by heterogeneous pools of neural stem cells (NSCs). Two distinct types of NSCs exist in the developing and adult mouse brain: Glial Fibrillary Acidic Protein (GFAP)-negative primitive (p)NSCs and downstream GFAP-positive definitive (d)NSCs. To better understand the embryonic functions of NSCs, we performed clonal lineage tracing within neurospheres grown from either pNSCs or dNSCs to enrich for their most immediate downstream neural progenitor cells (NPCs). These clonal progenitor lineage tracing data allowed us to construct a hierarchy of progenitor subtypes downstream of pNSCs and dNSCs that were then validated using single-cell transcriptomics. Further, we identify Nexn as required for neuronal specification from neuron/astrocyte progenitor cells downstream of rare pNSCs. Combined, these data provide single-cell resolution of NPC lineages downstream of rare pNSCs that likely would be missed from population-level analyses in vivo.

Keywords: primitive and definitive neural stem cells, neural progenitors, lineage analyses

Introduction

Single NSCs cultured in vitro are defined by their abilities to self-renew (produce secondary clonal colonies) and to produce the three differentiated neural cell types: neurons, astrocytes, and oligodendrocytes [1]. Primitive neural stem cells (pNSCs) are rare and do not express the canonical neural stem cell marker, *GFAP*, and thus are often missed in postnatal and adult studies that purify based on marker expression or sample a small number of cells [2,3]. Herein, we refer to *GFAP*-expressing NSCs as definitive (d)NSCs [4–6].

The two categories of brain NSCs (pNSCs and dNSCs) differ with respect to cell surface proteins [7,8], pluripotency markers [2,8], in vivo quiescence [3], and regenerative responses [3]. Indeed, post-natal clonal pNSC-derived neurospheres form by proliferation in leukemia inhibitory factor (LIF) whereas clonal dNSC-derived neurospheres form in fibroblast and epidermal growth factors with heparin (EFH). The two NSCs give rise to distinct proportions of oligodendrocytes, astrocytes, and neurons [2,8].

Of particular interest are the progeny of pNSCs, given that they would be missed by any general or *GFAP*-dependent lineage tracing, since pNSCs are rare Oct4-positive and Glial Fibrillary Acidic Protein (GFAP)-negative cells [9].

Previous studies on the specification of the neural progenitor cells (NPCs) downstream of the stem cells have concluded that they are generally unipotent (i.e., produce only neurons or only glial cells), particularly after E14.5–15.5 [10–12]; however, these studies and others found some proportions of clones with mixed progeny, suggesting that multipotent progenitors do exist [13–16].

Conversely, evidence for NPCs that are bipotent in glial lineages is less well documented: Temple and Raff reported a mixed astrocyte and oligodendrocyte precursor in the early postnatal optic nerve [17], and Vaysse and Goldman reported some cells from the newborn rat forebrain that can produce cells positive for the oligodendrocyte marker O4 as

[1]Department of Molecular Genetics, University of Toronto, Toronto, Canada.
[2]Center for Systems Biology, Lunenfeld-Tanenbaum Research Institute, Mount Sinai Hospital, Toronto, Canada.
[3]Institute of Medical Science, [4]The Donnelly Centre and [5]Department of Surgery, University of Toronto, Toronto, Canada.

well as the astrocyte/NSC marker GFAP [18]. More common in the literature are reports of NPCs of mixed neuronal and astrocyte or neuronal and oligodendrocyte lineages [11,14,19–21].

Here, we show by clonal lineage tracing, proliferation analyses, and single-cell transcriptomics that pNSCs and dNSCs give rise to distinct NPCs that have unique developmental trajectories en route to yielding post-mitotic forebrain cell types. Further, pNSC-derived NPCs appear less committed and more flexible in their transcriptional profiles, which suggest less lineage restriction than previously thought in these rare precursor cells. Last, using siRNA knockdown, we show that Nexn is found to be required for specification, but not maturation, of neuronal precursors downstream of bipotential neuron/astrocyte clones derived from pNSCs.

Methods

Mouse strains

All experiments were performed under the approval of the Animal Care Committee of the University of Toronto. Unless otherwise indicated, experiments were performed on E17.5 CD1 embryos. C57BL/6 and CD1 mice were purchased from Charles River (Wilmington, MA). CD1 mice were chosen because outbred mice have more genetic diversity, are more robust, and produce larger litter sizes than inbred mice. Tg(*GFAP-GFP)* mice were purchased from Jackson (Bar Harbor, ME; #010835). $GFAP^{TK}$ mice were a kind gift from Dr. M. Sofroniew [22].

Primary dissections and neurosphere cultures

The neurosphere assay was performed as previously described [23]. In brief, pregnant animals were anesthetized with isoflurane, the uterine horns removed and placed into cold artificial CSF. Embryos were cut out from uterine tissue and decapitated. After opening the skull and peeling back the cortex, the walls of the lateral ventricles were cut out from the forebrain and placed in serum-free media (SFM) for dissociation into single cells through mechanical dissociation.

Cells were plated in SFM (made in-house from GIBCO Dulbecco's modified Eagle's medium and F12) supplemented with either LIF (10 ng/mL) (recombinant) for growing pNSCs, or EGF (20 ng/mL; Sigma E4127), basic FGF (bFGF2, 10 ng/mL; Sigma F0291), and heparin (2 μg/mL; Sigma H3149) for growing dNSCs. Cells were plated in 24-well culture plates (Nunclon) in SFM with EFH at a density of 10 cells per microliter, which was previously shown to be sufficiently low density for growing clonal neurospheres [24] or up to 40 cells per microliter in LIF since pNSC-derived neurospheres are much more rare.

The resulting neurospheres were counted after 7–10 days in vitro using stringent size criteria: primitive neurospheres were defined as 50 μm or larger in diameter and definitive neurospheres as 100 μm or larger in diameter. All experiments were repeated at least in triplicate.

Neurosphere differentiation & self-renewal assays

After 7 days in culture, neurospheres were individually picked and plated onto laminin-coated plates (50 ng/mL), and they were differentiated for 7 days in the presence of 1% fetal bovine serum (Life Technologies, Carlsbad, CA). Cells were fixed in 4% paraformaldehyde (PFA) (Sigma) at room temperature.

To test for self-renewal, individual neurospheres were picked, transferred to an Eppendorf tube containing 200 μL SFM with growth factors, triturated 30–50 times with a glass Pasteur pipette tip, and transferred into an additional 300 μL of media in a 24-well plate. The number of secondary neurospheres per primary neurosphere was counted after 7–10 days in vitro.

Immunocytochemistry

Neurospheres differentiated on laminin-coated plates and fixed as stated earlier for immunocytochemistry (ICC) were stored in St-PBS at 4°C. Cell cultures were permeabilized with 0.3% Triton-X in PBS for 5 min at room temperature to allow staining of internal proteins. Samples were blocked with 10% NGS (normal goat serum; Jackson Labs) in St-PBS for 1 h at room temperature. Primary antibodies were diluted in blocking solution at 4°C overnight for plated cells. Secondary antibodies were incubated again in blocking solution for 40 min at room temperature for differentiated spheres. Nuclei were counterstained with Hoechst 33258 (1:1,000; Sigma).

The primary antibodies were mouse anti-GFAP (Sigma; MAB3402, 1:400), mouse anti-O4 (Millipore, Billerica; MAB345, 1:200), rabbit anti-βIII tubulin (CST; D71G9, 1:500), chicken anti-GFP (Aves Lab; 1:1200), rat anti-CD200 (OX90) PE (eBioscience; 12-5200-82, 1:800), rat anti-CD63 Monoclonal Antibody (NVG-2) APC (eBioscience; 17-0631-82, 1:800), mouse anti-BrdU (Dako; Clone Bu20a M0744, 1:200), and rabbit anti-Ki67 (Abcam; ab15580, 1:500). Secondary antibodies included: 488 goat anti- chicken (Alexa; A11039, 1:400), 488 goat anti- mouse (Alexa; A11029, 1:400), 488 goat anti-rabbit (Alexa; A11034, 1:400), 568 goat anti- mouse (Alexa; A11031, 1:400), and 568 goat anti-rabbit (Alexa; A11036, 1:400). Nuclei were stained with Hoechst (Sigma; 33258, 1:1,000). Staining was visualized on an AxioVision Zeiss UV microscope and Nikon 200 microscope or Olympus Fluoview FV1000 confocal laser scanning microscope.

Drop-seq & single-cell analyses

Primary neurospheres grown separately in either LIF or EFH, as cited earlier, were dissociated to single cells through trituration with a small bore hole glass pipette, then carried on ice to the Drop-seq facility at Princess Margaret Genomics Centre for single cell capture, cDNA amplification, and sequencing library preparation [25]. Cells from pNSC-derived neurospheres were run separately from cells from dNSC-derived neurospheres so that the NPC lineages downstream of each NSC type could be investigated.

Libraries were sequenced on an Illumina NextSeq500 to a depth of 60,000 reads per cell. FASTQ sequencing reads were processed, aligned to the mouse genome (mm10), and they were converted to digital gene expression matrices as per the standard instructions (Drop-seq, McCarroll Lab).

To analyze the Drop-seq data, a modified analysis pipeline combining low-level data analysis using the computational work-flow described by Lun et al. [26,27] was used, with

shared nearest neighbor (SNN)-Cliq-inspired clustering and t-SNE projection using the Seurat R package. Data were visualized using scClustViz, as described earlier [28,29]. In brief, cell doublets were first filtered by fitting the library size of each cell to a negative binomial distribution and removing large libraries ($P \leq 0.001$). Next, contaminating cells (e.g., red blood cells from primary dissection) were removed by removing cells that were outliers in a correlation between library size and gene detection rate.

Third, dead cells were filtered out by mitochondrial gene content by computationally removing cells that were at least four median average deviations higher than the median mitochondrial transcript proportion at each time point using the scran package. Low-abundance genes were removed by computationally removing any gene that was found (unique molecular identifier expression value >0) in less than three cells.

Data were normalized using the default implementation of the Lun et al. [26] pool and deconvolute normalization algorithm in the scran package. This method is robust to the sparsity of the data and respects the assumption of minimal differential gene expression common to most normalization methods. Following low-level data analysis and normalization, data were transferred to a Seurat object and highly variable genes were used to carry out PCA. Using Seurat, principal components were used for clustering. T-SNE projections, cell cycle annotations, and differentially expressed genes were produced in R using the Shiny script.

Trajectory analyses were performed using p-Creode (https://github.com/KenLauLab/pCreode).

siRNA assays

The germinal zone of *Oct4*$^+$ E17 mice was dissected, and single cells were dissociated and plated in SFM supplemented with LIF for the neurosphere assay [23], where pNSCs and progenitors proliferated for 7 days. Cells were then differentiated using 1% fetal bovine serum for the next 7 days. The cultures were either left untreated in media only (control), were treated with non-targeting siRNA (control for any unwanted siRNA damage), or were treated with *NEXN* siRNA (to knock down *NEXN* gene expression).

These three treatments were added to the culture in proliferation stage only (first 7 days), differentiation stage only (last 7 days), or throughout both stages (all 14 days). The cells were subsequently fixed and ICC was performed with antibodies against the neuronal βIII and the astrocytic GFAP cell markers, whereas nuclei were counterstained with Hoechst, to quantify the amount of neurons and astrocytes produced from pNSC-derived progenitors.

Neurite length analysis

Neurite length was quantified using the Simple Neurite Tracer (SNT) plug-in on ImageJ as in Longair et al. [30]. Primary neurites were traced manually from the soma to the point of bifurcation or to the end of the outgrowth. Areas with overlapping neurite processes and neurites extending out of the image were omitted from SNT analysis.

Secondary neurites were traced manually from the point of bifurcation of the primary neurite up to the end of the outgrowth or to where the tertiary neurites bifurcated.

Results

Clonal retroviral lineage tracing of NPCs in vitro shows distinct specification of NPCs downstream of pNSCs versus dNSCs

Both primitive and definitive NSCs give rise to all three major cell types of the neural lineage across multiple ages in development and adulthood, though the proportions vary by age and between NSC types [2,8,9,31]. pNSC-derived neurospheres from the E17 forebrain germinal zone grown in LIF gave rise to roughly similar proportions of neurons and astrocytes as did dNSC-derived neurospheres grown in EFH (although there is a trend toward more neurons and fewer astrocytes produced by pNSCs) (Fig. 1A).

Significantly fewer O4+ oligodendrocytes are produced by pNSCs than dNSCs ($6.64\% \pm 1.07\%$ of Hoechst+ cells vs. $15.70\% \pm 0.74\%$, $P < 0.01$ by *t*-test; Supplementary Fig. S1A). Individual pNSC-derived neurospheres could be dissociated and passaged into LIF or EFH demonstrating self-renewal and downstream lineage competency, respectively (Fig. 1B), though note that dNSC-derived neurospheres cannot give rise to pNSC-derived neurospheres [2].

Lineage specification of precursors at age E17 in mouse brain development is of particular interest since that is when forebrain precursors switch from high levels of neurogenesis

FIG. 1. Clonal lineage tracing in vitro with RV-GFP reveals different proportion of unipotent and bipotent cells downstream of pNSCs and dNSCs. **(A)** Differentiation profile of pNSC-derived NS grown in LIF and dNSC NS grown in EFH from the E17.5 brain germinal zone. $n \geq 4$ NS per marker, $P < 0.01$ **(B)** Individual pNS-derived NS can be passaged into LIF or EFH. $n \geq 45$ NS per condition. **(C)** Strategy for clonal retroviral lineage tracing of primitive and definitive NS. Average percent of clones **(D)** and number of cells per clone **(E)** with given composition for RV-GFP tranductions on day 2, 4, or 6 are shown. **(F)** Astrocytes were primarily identified by GFAP immunostaining and secondarily by large star-shaped morphology as illuminated by GFP expression. Neurons were marked by βIII-tubulin immunostaining and a small round nucleus, often with two neurites more than double the length of the nucleus. Oligodendrocytes were rarely scored by morphology, and when they were it was based off presence of radial ''end feet.'' White asterisks indicate an unstained cell scored as an oligodendrocyte. Red asterisk denotes a cell that would be classified as an astrocyte by morphology. *Yellow arrowheads* clarify examples of GFP$^+$BIII$^+$ cells. *Blue* = Nuclei; *Yellow* = neurons; *Red* = astrocytes; *Green* = Cells infected by RV-GFP. **(G)** Breakdown of number of cells per of clones as per **(E)**. For pNSC-derived clones, 1-way ANOVA $F(4,44) = [4.192]$, $P < 0.01$) for pNS, followed by Tukey's Multiple-Comparison Test. For dNS clones, $F(4,82) = [8.377]$, $P < 0.0001$, followed by Tukey's Multiple-Comparison Test. At least 8 NS and up to 44 were used for each lineage tracing time point at day 2, 4, or 6. $^*P < 0.05$, $^{**}P < 0.01$, $^{***}P < 0.001$. pNSC, primitive neural stem cell; dNSC, definitive neural stem cell; GF, growth factor; GFAP, Glial Fibrillary Acidic Protein; RV-GFP, retrovirus encoding GFP; LIF, leukemia inhibitory factor; EFH, epidermal growth factors with heparin; NS, neurospheres.

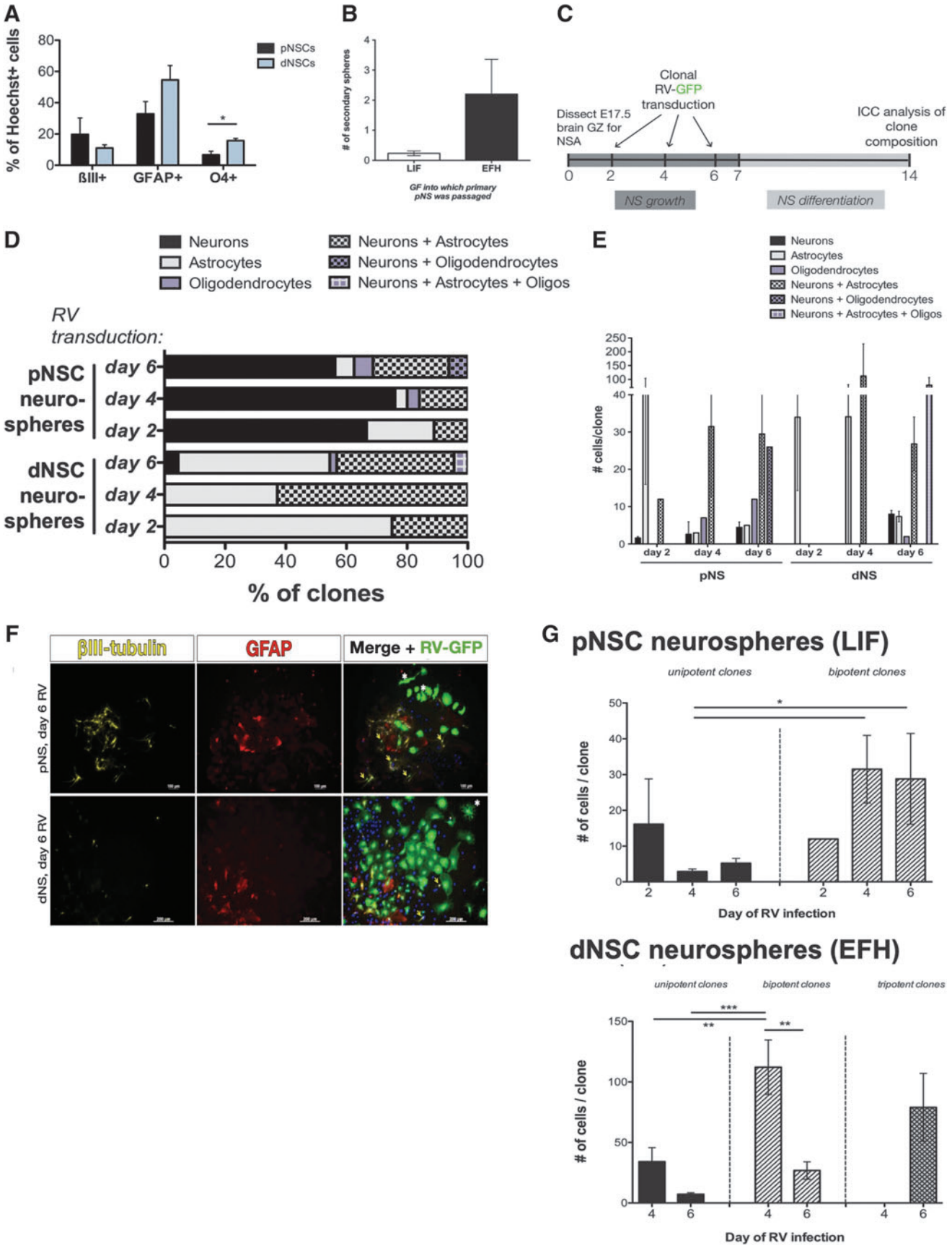

to greater astrogenesis [32–34]. Hence, to further explore the differences in NPCs most directly downstream of pNSCs and dNSCs, clonal lineage tracing was performed during primary neurosphere formation in LIF or EFH, respectively. The advantage of conducting this experiment in vitro is that we could exploit the clonal neurosphere assay to query the most immature NPCs, particularly those directly downstream of the rare pNSCs, which make up less than 0.01% of the germinal zone cells in vivo [2].

A clonal titer of a retrovirus encoding GFP (RV-GFP) was administered on either day 2, 4, or 6 of the neurosphere growth, and neurospheres were picked for differentiation on day 7 (Fig. 1C) by plating them down in 1% serum for an additional 7 days. The following two criteria define clonal titers in these experiments, making it statistically unlikely that more than one cell was ever infected: (1) fewer than 50% of neurospheres assayed should have any GFP^+ cells, and (2) the average # of cells infected per well should be less than two at 36 h after retrovirus infection.

Cell fates were determined by ICC in addition to strict morphological criteria (Fig. 1D, F). Three clear patterns emerged comparing clones downstream of pNSCs and dNSCs: (1) most pNSC-NPC clones contained only neurons, and less than half were bipotent in nature, compared with very few neuron-only clones downstream of dNSCs; (2) approximately equal numbers of dNSC-NPC clones contained only astrocytes or were bipotent (contained both astrocytes and neurons); and (3) regardless of date of infection, clones of mixed fates were statistically larger in size than unipotential clones (Fig. 1E, G).

To test whether this was due to the difference in growth factors or an intrinsic difference in the two types of stem cells, we switched the growth factors (from LIF to EFH, or vice versa from EFH to LIF) at day 5 of neurosphere growth. This did not impact fate specification (Supplementary Fig. S1B), as evidenced by the presence of more neuron-only clones and fewer astrocyte-only clones from the original pNSCs compared with the original dNSCs (Supplementary Fig. S1C).

Mixed clones containing neurons and astrocytes usually had one dominant cell type within each clone. This, in addition to the smaller size of unipotent clones, suggests a lineage restriction model whereby progenitors commit to a fate as they divide rather than remain bipotent.

Many clones contained both βIII-tubulin+ neurons and $GFAP^+$ astrocytes, whereas no clones contained both $GFAP^+$ astrocytes and oligodendrocytes. One clone was found in pNS-derived colonies that contained βIII+ neurons and $GFAP^-/\beta III^-$ oligodendrocytes, identified by morphology. Two clones (containing 51 and 107 cells) from dNSC-derived neurospheres infected on day 6 of the neurosphere assay gave rise to all three major cell types.

Given the rarity of this multipotent clone (2/44 or 4.5% of dNSC-derived clones) and larger size (reflecting more proliferative ability of the initial cell), the initially infected cell may have been a dNSC rather than a tripotent progenitor. Perhaps the most surprising result from these analyses is the predominance of neuron-only clones downstream of pNSCs and the predominance of astrocyte-only clones downstream of dNSC-derived neurospheres.

pNSCs can give rise directly to NPCs without a dNSC-intermediate

Although pNSCs do not express GFAP, they do give rise to *GFAP*-expressing cells, including dNSCs [2,8]. Therefore, we sought to determine the number of $GFAP^+$ cells within pNSC-derived neurospheres by flow cytometry using Tg(*GFAP-GFP*) adult mice. In contrast to dNSC-derived neurospheres that were found to contain 74.1% GFP^+ cells, pNSC-derived neurospheres contained 48.8% GFP^+ cells based on gates set by a negative control (Fig. 2A).

To investigate whether pNSCs directly give rise to differentiated post-mitotic progeny or always divide to produce a $GFAP^+$ dNSC intermediate, mice with the herpes simplex virus tyrosine kinase under control of the *GFAP* promoter ($GFAP^{TK}$ mice) were used, enabling the selective ablation of proliferating GFAP-expressing cells [2,8,22,35].

On exposure to the drug ganciclovir (GCV), *GFAP*-expressing cells that express the viral TK metabolize GCV to toxic GCV triphosphate, which is both a competitive inhibitor of dGTP and serves as a poor substrate for chain elongation. This allows for selective toxicity only in *GFAP*-expressing cells that are also synthesizing DNA in preparation for division.

We used postnatal day (PND)7 $GFAP^{TK}$ mice and their littermate controls, a time when *GFAP* is expressed in the germinal zone, and then pNSC- and dNSC-derived neurospheres were grown clonally either with or without GCV (Fig. 2B). The number of EFH neurospheres from $GFAP^{TK}$ mice were greatly reduced in the presence of GCV, as expected since EFH neurospheres are clonally derived from *GFAP*-expressing dNSCs.

The numbers of adult pNSC-derived pNSC-derived neurospheres from $GFAP^{TK}$ mice were unaffected by GCV

FIG. 2. Identification and knockdown of *GFAP* expression in pNSC and dNSC progeny. Density plots of GFAP-GFP cells from dissociated pNSC-derived **(A)** and dNSC-derived NS after 7 days of sphere growth in vitro, with negative gating set by a CD1 negative control (not shown). **(B)** Percentage of pNSC- and dNSC-derived NS from GFAP-TK mice grown in LIF or EFH, respectively, with or without GCV, which kills dividing cells expressing the herpes simplex virus thymidine kinase from the *GFAP* promoter. Percentage of spheres normalized to number of NS grown in the absence of GCV from GFAP-TK mice. $n = 11$ mice across three experiments. Two-way ANOVA shows a significant interaction ($F = 15.52$, $P < 0.001$). $^*P < 0.05$ and $^{***}P < 0.001$ by Bonferroni post-test. **(C)** Average percentage of $GFAP^+$ and $\beta III\text{-tubulin}^+$ cells in pNSC-derived NS from GFAP-TK mice grown and differentiated with or without GCV, normalized to the no GCV control. Two-way ANOVA shows a main effect of GCV ($F = 6.784$, $P < 0.01$). $^*P < 0.05$ by Bonferroni post-test. **(D)** Sample wells of differentiated pNSC NS from the same GFAP-TK mouse showing the loss of neurons with the addition of GCV. **(E)** Average percentage of $GFAP^+$ and $\beta III\text{-tubulin}^+$ cells in dNSC-derived NS from GFAP-TK mice grown and differentiated with or without GCV, normalized to the no GCV control. Two-way ANOVA shows a main effect of GCV ($F = 30.01$, $P < 0.0001$), $^{**}P < 0.01$, $^{***}P < 0.001$ by Bonferroni post-test. $n \geq 8$ NS per genotype and condition. Error bars reflect standard error of the mean. GCV, ganciclovir.

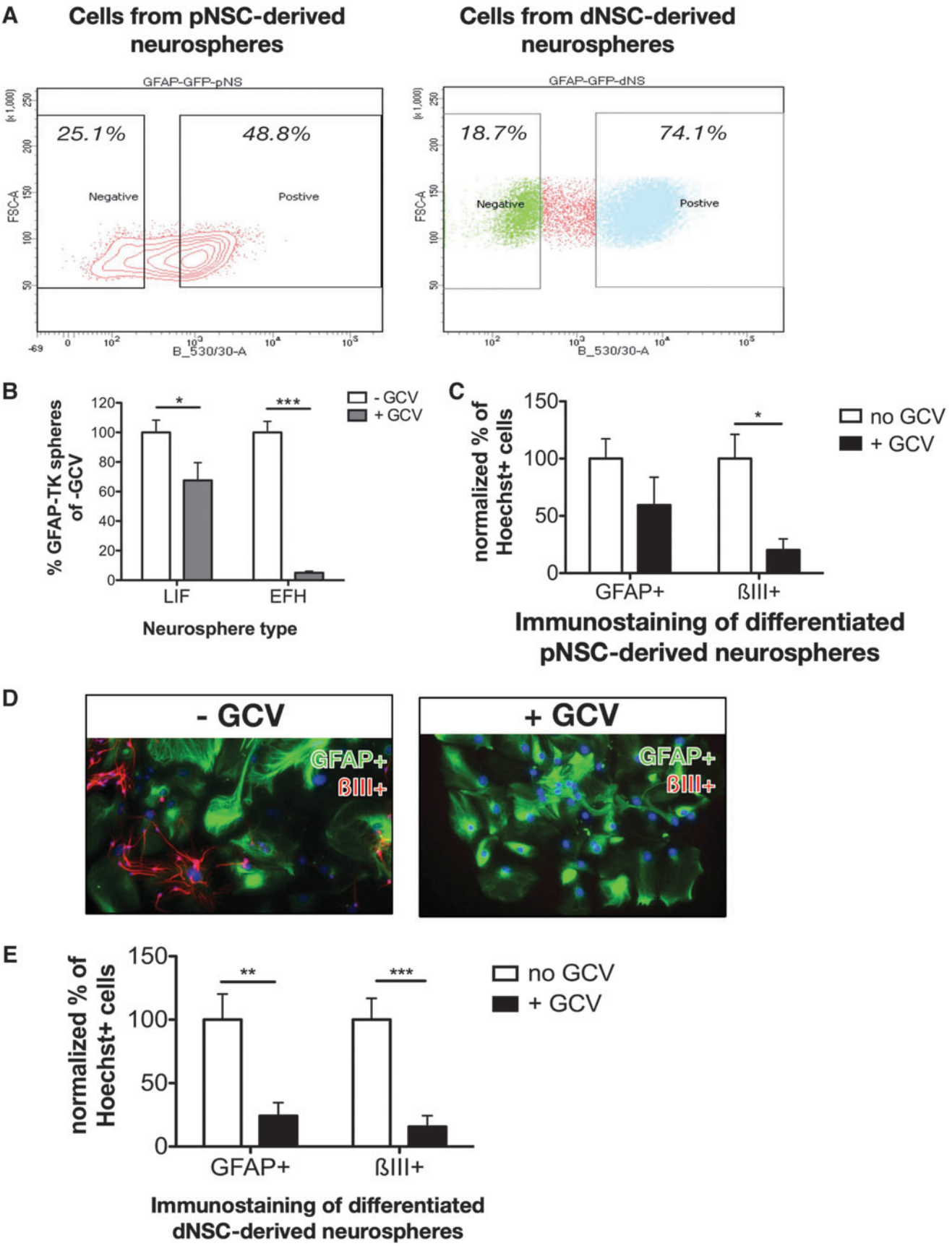

exposure [2], whereas the numbers of *GFAP*^{TK} PND7 pNSC-derived neurospheres were slightly reduced in GCV, suggesting that a subpopulation of pNSCs may co-express *GFAP* in the postnatal period. This finding could reflect a transition period where pNSCs are transitioning to dNSCs.

Most surprising, primitive neurospheres from *GFAP*^{TK} animals grown and differentiated in GCV can still generate GFAP^{+} astrocytes, but only produce 20% of the control number of neurons (–GCV condition) (Fig. 2C, D). Conversely, dNSC-derived neurospheres grown in the same GCV conditions make only small numbers of either neurons or astrocytes (Fig. 2E). This suggests that pNSCs primarily give rise to neurons via an intermediate that is both dividing and expressing *GFAP*, which could include GFAP^{+} NPCs or dNSCs.

However, given the observed rarity of dNSCs downstream of pNSCs in pNSC-derived neurospheres (based on passaging data) (Fig. 1B), these neurons are more likely derived from GFAP^{+} NPCs. Thus, pNSCs that do not express *GFAP* themselves must give rise to downstream proliferating GFAP^{+} progenitors on their way to making most of their postmitotic neuronal progeny.

Hierarchical model of NPC subtypes

Based on the lineage tracing and *GFAP*^{TK} results, a hierarchy of NPCs downstream of pNSCs and dNSCs was created with the simplest number of progenitors and branches (Fig. 3). The fate and position of NPCs in this hierarchy are derived from the RV clonal lineage tracing experiment. For example, clones that were large and bipotent are represented by an NPC in the hierarchy toward the top, giving rise to other NPCs that eventually give rise to two distinct fates.

Notably, since most neuron/astrocyte mixed clones from primitive neurospheres contained more of one cell type than the other, there may be two types of neuron/astrocyte bipotent NPCs downstream of pNSCs, indicating specification biases. As shown in Fig. 3, the following six unique types of progenitors were observed: (1) Unipotent astrocyte NPC; (2) Unipotent neuronal NPC; (3) Unipotent Oligodendrocyte NPC; (4) Bipotent Neuronal/Astrocyte (Neuron-enriched) NPC; (5) Bipotent Neuronal/Astrocyte (Astrocyte-enriched) NPC; and (6) Bipotent Neuronal/Oligodendrocyte NPC.

Interestingly, although many NPC types were seen downstream of both pNSCs and dNSCs, the bipotent neuron/oligodendrocyte NPC and bipotent neuronal/astrocyte (neuron-enriched) NPC were exclusive to the pNSC lineage. We observed no bipotent oligodendrocyte/astrocyte NPCs downstream of either NSC type. We cannot determine whether the very few tripotent clones observed were a result of infecting a dNSC or a tripotent NPC.

The lack of unipotent NPCs directly downstream of pNSCs is consistent with the larger size of bipotent clones. The finding that significantly fewer neurons were made from *GFAP*^{TK} pNSCs grown in the presence of GCV supports the idea that neurons are generated from pNSCs via a progenitor that expresses *GFAP* while it is proliferating. However, whether this cell is the bipotent neuronal/astrocyte progenitor or the unipotent neuronal progenitor, cannot be determined.

Single-cell transcriptomics on precursor populations validates hierarchical model generated with lineage tracing

To determine whether there are unique molecular markers for the functionally distinct NPCs downstream of pNSCs, single-cell RNA Drop-seq was used [25]. Primary cells from the E17 forebrain germinal zone were grown as clonal spheres for 7 days in either LIF or EFH, and then dissociated to single cells for Drop-seq analyses. The relative expression

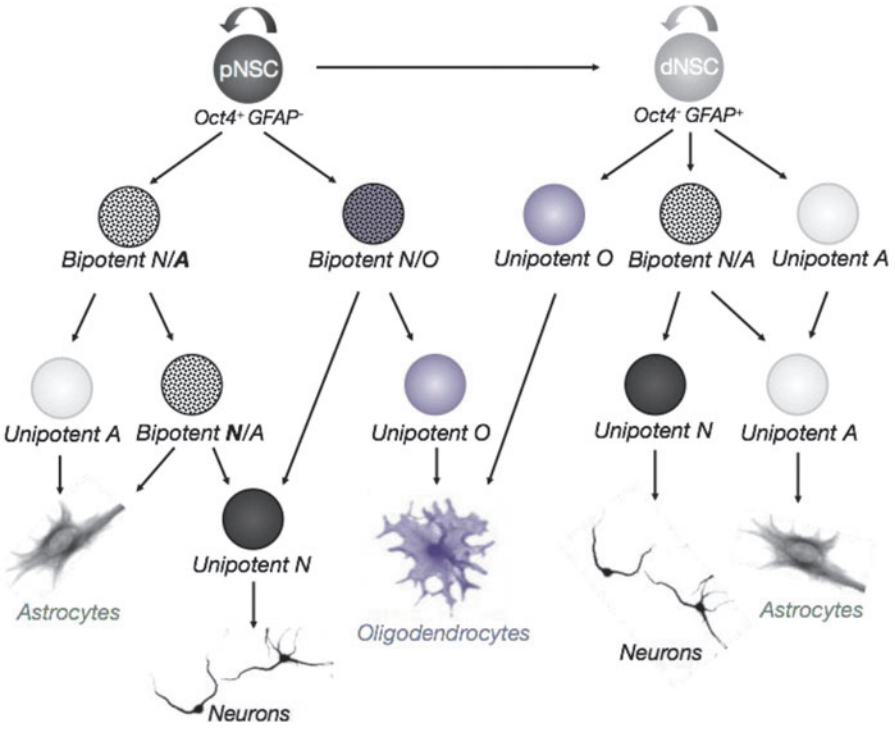

FIG. 3. Proposed NPC lineage. NPCs are the spheres lacking *curved arrow* above signifying self-renewal, color-coded based on the fate of daughter cells. *Gray* cells are bipotent astrocyte progenitor cells that can make both neurons and astrocytes. *Light gray* cells are unipotent astrocyte progenitors. *Black* cells are neuronally-specified progenitors. *Dark purple* cells are bipotent neuron and astrocyte progenitors, and *light purple* are oligodendrocyte progenitors. The *blue background* highlights NPCs that are unique between pNSCs and dNSCs. A = Astrocyte, *N* = Neuron, O = Oligodendrocyte, N/A = neuron/astrocyte bipotential progenitor that is enriched for neurons, N/A = neuron/astrocyte progenitor that is enriched for astrocytes.

of several known NSC/NPC markers and established differentially expressed genes were visualized on the t-SNE plot, allowing for a general characterization of five distinct clusters (Fig. 4A).

We found that 100% of cells in Cluster 5 expressed Top2a, and 85% expressed Ki67 and Sox2, markers of proliferation and proliferative neural precursors. We focused on the proliferating cells in cluster 5 since they comprise the proliferative precursors that would have been sampled in the RV-GFP lineage tracing experiment, given that retroviruses require cell division to be incorporated.

Using candidate markers for NPCs and by performing subset analyses to identify differentially expressed genes between subregions of cluster 5, four potential subtypes of proliferating NPCs were observed (Fig. 4B). These subtypes correspond to the different NPC types predicted by the lineage tracing clonal analyses (Fig. 1D). $Ki67^+$ cells comprising the horizontal arm of cluster 5 expressed common astrocyte markers such as Fabp7, Mt8, and Aqp4; the diagonal component of cluster 5 expressed the neuronal markers Dcx, Brn2, and Dlx2 (Supplementary Fig. S2A). Dlx2 The marker expression in these clusters is consistent with unipotent astrocyte or neuronal NPCs, respectively.

Conversely, cells at either end of the horizontal branch expressed a combination of markers for neuronal and astrocyte fates, consistent with bipotent NPCs producing different ratios of neurons and glia (since very few bipotent clones contained equal ratios of neurons to astrocytes). The convergence point between the two axes may represent the neuron-enriched bipotent NPCs, whereas the bipotent edge at the end of the astrocyte arm would be the bipotent astrocyte-enriched NPC.

Cluster 5 contained Ki67+ precursors, whereas cluster 4 expressed glial markers, including subclusters for astrocytes and oligodendrocytes (Supplementary Fig. S2B, C). Of note, clusters 1, 2, and 3 all contained predominantly neuronal markers (Fig. 4C). Transcripts for *Dlx2*, a marker of proliferating as well as migrating GABAergic interneurons, were found in clusters 2 and some of cluster 3, suggesting that those clusters contain the early neuronal progenitors made from proliferating precursors in cluster 5. *Arx* transcript – another marker of cell migration – was present in far more cells from cluster 3 compared with cluster 1.

Foxp1, a marker for GABAergic medium spiny projection neurons of the striatum, was differentially expressed in cluster 1, suggesting an overall counter-clockwise gradient of maturation in the upper part of the t-SNE plot. These trends were confirmed by statistical analyses through a series of pairwise tests (Fig. 4D).

A subset analysis of the largest density in cluster 1 and the majority of cluster 3 (Fig. 4E) revealed that cluster 3 has many migratory neuronal precursors, whereas cluster 1 has more specified precursors for medium spiny and pyramidal neurons (based on differential expression of Foxp1).

Since cluster 1 was large and seemed to contain cells mostly specified to be neurons, we performed an additional subset analysis on the densities of cells visually identified to determine whether there were more differentially expressed genes that may be indicators of different neuronal subtype precursors missed in the larger comparison and not addressed by the ICC performed after lineage tracing in vitro.

The analyses revealed that the smaller density (denoted set B in Fig. 4F) contained more genes for axonal growth, as well as Sstr1 (marker of medium spiny neurons of the striatum [36]) and Thsd7a, which marks motor neurons in zebrafish [37]. The larger group of cells in cluster 1 (Set ''A'') contained cells that expressed GABAergic and Glutamatergic pathway transcripts, including many cells with co-expression of both, suggesting that single neural stem cells may make many types of neurons. Thus, many of the progenitor cell types discovered in the retroviral lineage analyses may be consistent with progenitor cell types emerging from the single-cell transcriptomics.

Primitive neurosphere trajectory analyses show a distinct pathway for olfactory bulb interneuron NPCs

We next took advantage of p-Creode, an algorithm for mapping state transitions and identifying consensus routes

FIG. 4. Single-cell RNA-sequencing of pNSC-derived NS using Drop-seq. **(A)** t-SNE plot to visualize cells from pNSC-derived NS run through Drop-seq, showing five major clusters. Each individual *dot* reflects a single cell, and the colours denote cluster membership. **(B)** Magnification of proliferative cells within *Top*$2a^+$/$Ki67^+$ cluster 5, with canonical markers for astrocytes (Aldh1l1, Aqp4, Mt8, Fabp7) and neurons (Dcx, Brn2, Sp8, Dlx2) showing stratification of putative neuronal versus astrocyte-specified progenitors. Overlap of expression is seen at the corners in boxes, and thus these are proposed to represent bipotent neuron/astrocyte NPCs. The bipotent NPC's enrichment for astrocytes versus neurons is hypothesized based on proximity to glial versus neuronal NPCs and candidate expression. **(C)** Overlay of candidate markers reveals general cluster identities. *Yellow* is low/no expression, and *green*/*blue* represents high expression. GFAP represents dNSCs and/or astrocytes is largely confined to cluster 4; Dlx2 marks migrating subpallial progenitors in clusters 2 and 3; Foxp1 marks medium spiny neurons of the cortex and striatum, and is confined to cluster 1; and Ki67 is a proliferation marker confined to the smallest cluster, number 5 (confirmed by Cyclone analysis of cell cycle phase on the far *right*). Cyclone analysis color-codes cells by phase of cell cycle: G1 (*yellow*), G2M (*purple*), and S phase (*green*). The majority of cells are in G1, with the dramatic exception of cluster 5. **(D)** Dotplot showing genes positively differentially expressed versus all other clusters in a series of pairwise tests (Wilcoxon rank-sum tests with a 1% false detection rate threshold). The size of the *dot* encodes the detection rate (proportion of cells expressing the gene), and *dot* color shows the average gene expression level for cells within the cluster (as per key in *lower left*). Clusters are marked on the *left* with the number of positively DE genes listed, and a dendrogram illustrating cluster similarity. The dendrogram along the *top* of the *dot* plot reflects gene expression similarity, with gene names along the *bottom* of the dotplot. **(E)** Subset analyses based on *Foxp1* expression (Set A) and $Dlx1^+$ cluster 3 cells (Set B) confirm that cluster 3 cells are migratory neuronal precursors. **(F)** Subset analyses between subclusters within cluster 1 suggest putative neuronal subtype differences within subclusters, such as $Thsd7a^+$ neurons. t-SNE, t-distributed stochastic neighbor embedding; DE, differentially expressed.

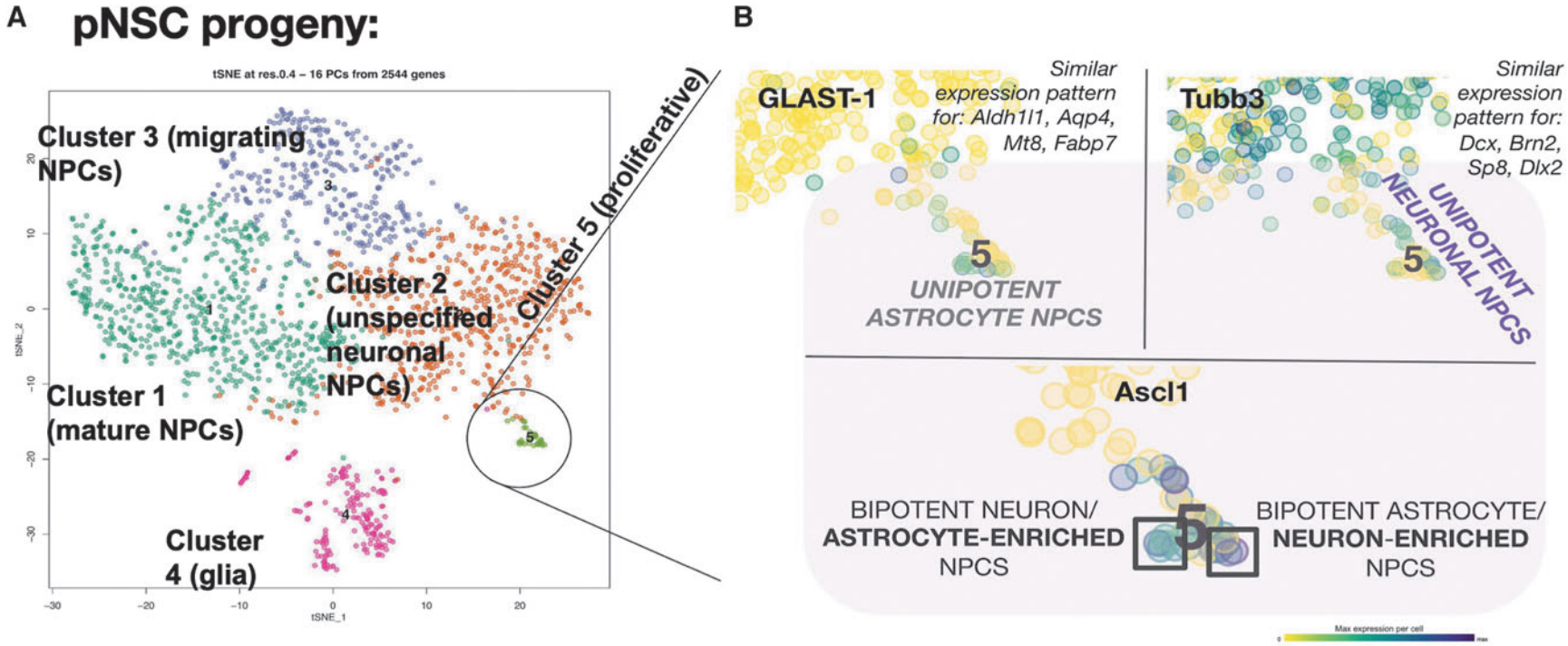

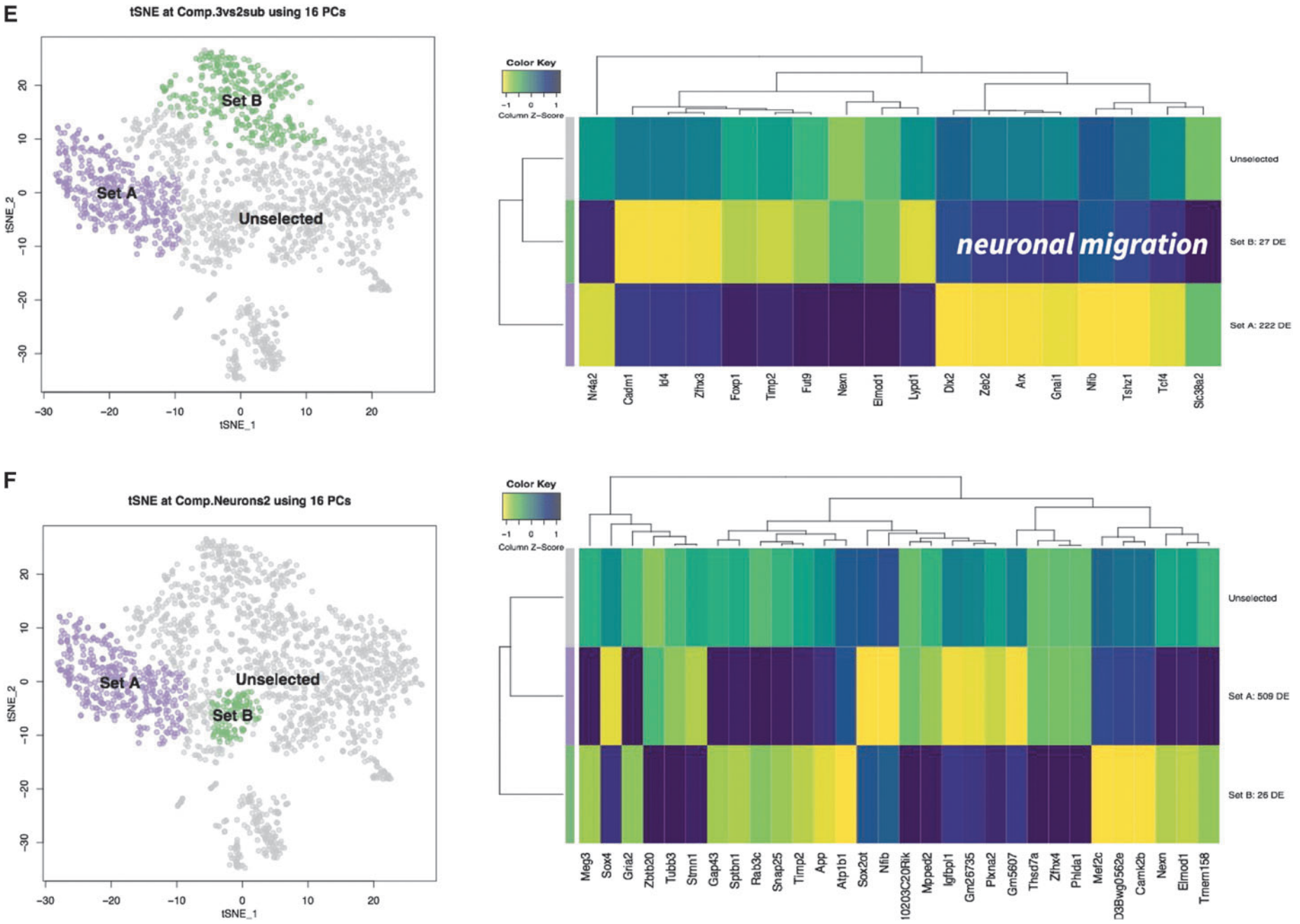

FIG. 4. (*Continued*).

from single-cell data [38], for lineage analysis. Figure 5a shows the lineages of cells downstream of pNSCs identified by p-Creode. Each circle represents a set of transcriptionally-related cells, with the size of the circle reflecting the number of cells in the set and the color reflecting the clusters previously identified in Fig. 4.

Notably the smaller clusters 4 and 5, glial and proliferative clusters, respectively, in Fig. 4A and B are interspersed between the large clusters 1 and 2, as in the p-Creode mapping of the same data (Fig. 5). Indeed, overlaying candidate genes used to categorize subtypes of neurons made by germinal zone precursors identified distinct developmental trajectories of progenitors that give rise to striatal medium spiny neurons (marked by Darpp-32, Foxp1, and Sstr2 expression), GABAergic olfactory bulb interneurons (marked by Sp8, Sall3, and Pvalb expression), and oligodendrocytes (marked by Mbp and Sox10 expression), with markers for astrocytes (e.g., Aqp4, Gfap, and Slc1a3) and cortical interneurons (e.g., Npy, Tac1, Ssp) interspersed among some of these trajectories.

Of interest, a distinct pathway for progenitors that only express candidate markers of olfactory bulb interneurons was observed (Fig. 5, to the right of putative point of origin), but these markers also are expressed in trajectories for other neuronal subtypes. This may mean that (1) olfactory bulb interneurons can be made both via common and unique progenitors, or (2) there is an initially common neuronal progenitor downstream of pNSCs that has an early fate branchpoint for olfactory bulb (OB) versus non-OB cell types, though progenitors destined to make non-OB neuronal cell types continue to express genes for olfactory bulb interneurons after the branch point and would presumably shut down expression over time.

NPCs require Nexn for neuronal specification

We examined the mature NPCs in cluster 1 in further detail to learn how pNSCs may generate neurons. Our analysis using scClustViz [28] identified Nexilin (Nexn) and Lphn2 to be potential specific marker genes for neuronally specified precursors (cluster 1; Fig. 4D). We focused on Nexn because of its relative specificity for this cluster and high differential expression.

Nexn is an actin-binding protein that has been shown to function in cell adhesion during cell migration [39], but it has not been previously described in the context of NPCs. To test for its potential functional significance in specifying the neuronal fate in NPCs, we administered siRNA targeting Nexn transcripts during the 7 days of pNSC sphere formation in LIF (Fig. 6A and Supplementary Fig. S3A, 85% knockdown compared with non-targeting siRNA control by qPCR), followed by 7 days of differentiation in 1% FBS without siRNA.

As predicted based on Nexn's selective expression in the mature NPC cluster 1 (Fig. 6B), significantly fewer ßIII+ neurons formed when Nexn were knocked down during NPC proliferation and neurosphere formation compared with control conditions with no siRNA (Fig. 6C), whereas astrocyte numbers were unchanged across all conditions (Fig. 6D).

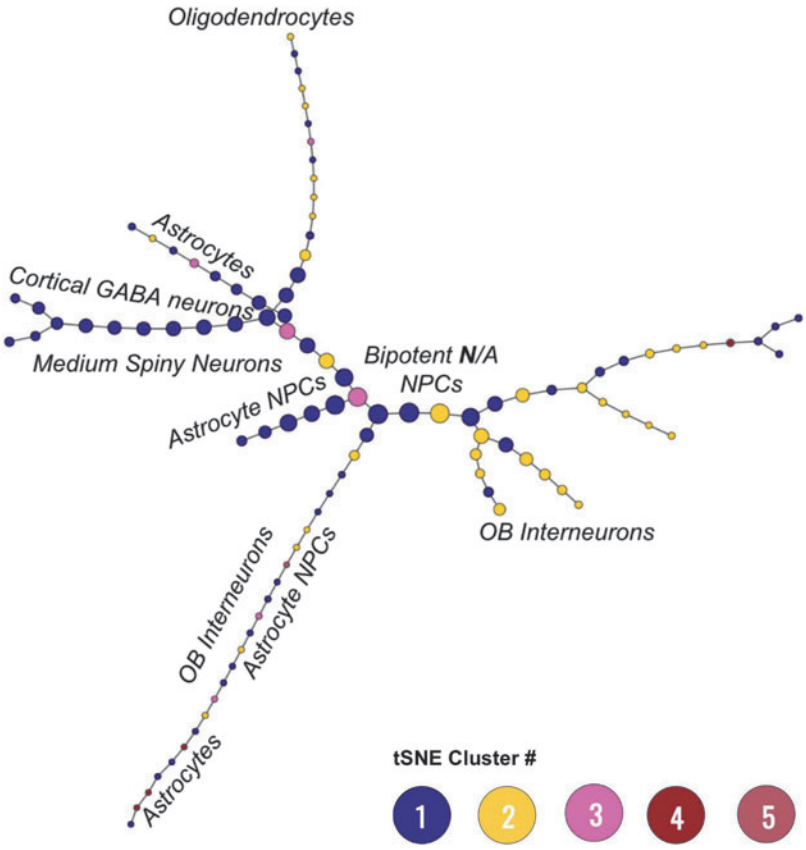

FIG. 5. p-Creode corroborates distinct OB interneuron NPCs downstream of pNSCs. Unsupervised lineage analysis of pNSC-derived progeny using p-Creode. Circles represent nodes of cells (>1 cell per node), with the size of each node reflecting the number of cells it contains, and color representing Seurat clusters as in key. The lines connecting nodes represent lineage relationship between groups of cells. The small diagram in the bottom left reflects each node's average expression of Ki67, where warm tones are high expression and cold tones low.

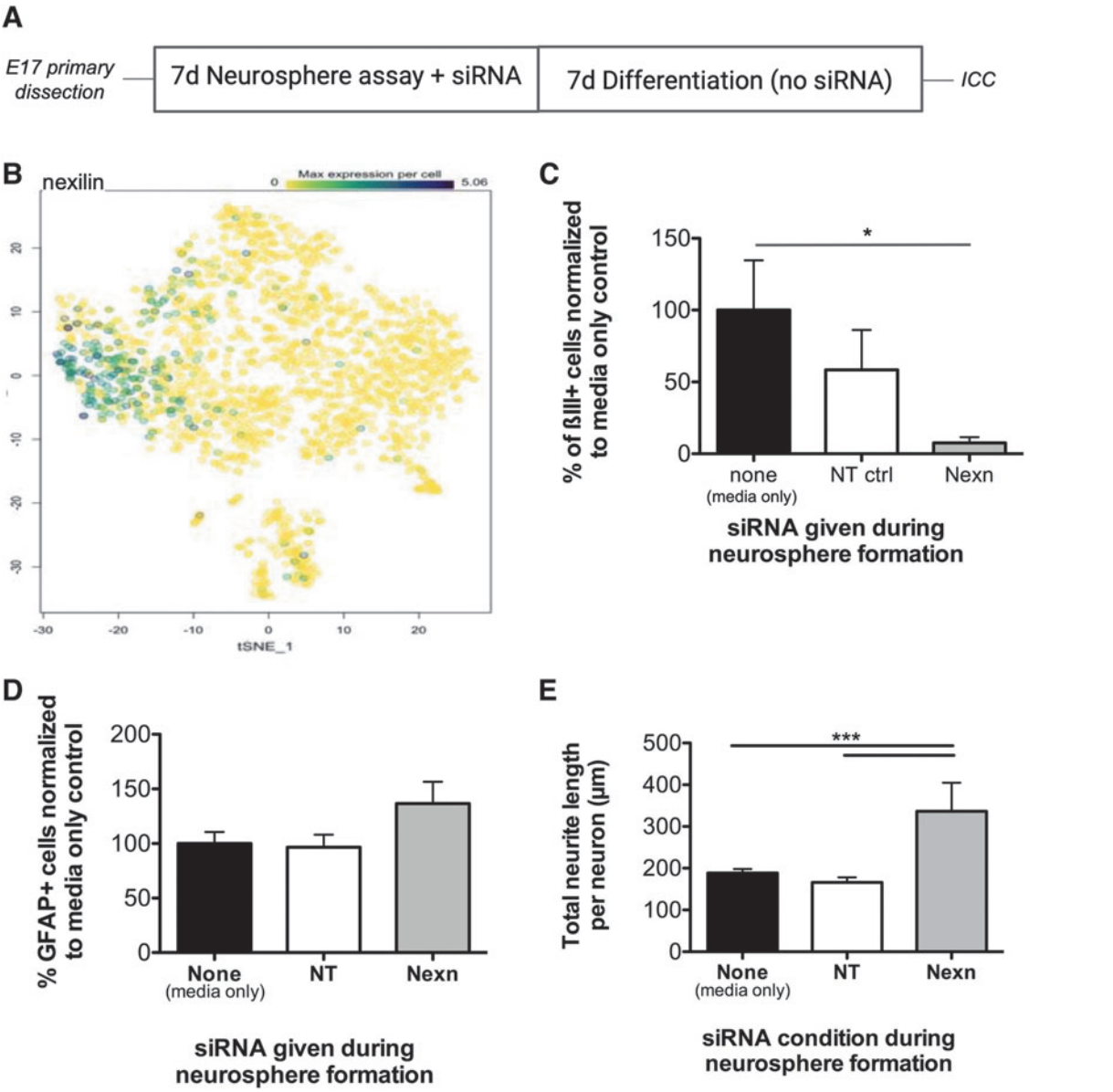

FIG. 6. Nexn is required for specification, not maturation, of neuronally specified progenitors downstream of pNSCs. **(A)** Protocol for siRNA-mediated knockdown of Nexn during neurosphere formation, but not differentiation, to test the role of Nexn in neuronal progenitor specification. **(B)** Overlay of Nexn expression on t-SNE, where blue/green denotes higher differential expression. Knockdown of Nexn during neurosphere formation leads to fewer neurons **(C)** but no change in the proportion of astrocytes **(D)**. $n = 7$ wells per condition for βIII stained wells and $n = 4$–6 wells for GFAP stained wells. For **(C)**, $F(2,18) = [3.227]$, $P < 0.01$, with * reflecting $P < 0.05$ for None versus Nexn by Dunnett's Multiple-Comparison Test. **(E)** Neurite length for βIII^+ cells was measured using Single Neurite Tracer. $n = 103$ neurons for media-only condition, 50 neurons for NT siRNA control condition, and 13 neurons in the Nexn siRNA condition. One-way analysis of variance, $F(2,163) = [12.11]$, $P < 0.0001$, with *** reflecting $P < 0.0001$ on Tukey's Multiple-Comparison Test. Errors bars reflect standard error of the mean. NT, non-targeting.

The finding that Nexn knockdown during the neurosphere growth phase (and not during the differentiation of post-mitotic cells) resulted in a loss of neurons suggests that Nexn is required for neuronal specification before post-mitotic differentiation. We next asked whether Nexn was also required for neuronal maturation by performing a neurite length analysis on the few new neurons that did persist during Nexn knockdown.

We found that the total neurite length per neuron was on average longer than in control conditions (Fig. 6E), consistent with the hypothesis that Nexn is not required for neuronal maturation but rather for specifying the neuronal fate. There were no significant changes in the average number or length of secondary neurites, further supporting this conclusion (Supplementary Fig. S3B, C). The increase in neurite length after Nexn knockdown might reflect an

indirect, non-cell autonomous effect of having fewer neurons competing for growth factors in the knockdown condition.

Discussion

Although both pNSCs and dNSCs are multipotent for neural cell types, the similarities between their progeny and the extent to which they are lineage-restricted has not been fully understood, though this lineage restriction process is critical for the formation of the functional units of the brain. Understanding the lineages downstream of either NSC type can not only identify novel targets for endogenous regenerative strategies, but more broadly help answer the question of how the diversity of cell types of the mature brain arises.

The lineage of pNSCs is of particular interest given their very early embryonic development [40,41], rarity in vivo in the adult [3], and their significant contribution to brain development [9]. Further, pNSCs have been shown to contribute to the regenerative capacity of the germinal zone following ablation of dNSCs in the adult mouse brain [3], and they show early responsiveness to brain injuries such as stroke [2]. Indeed, pNSCs can be derived from the embryonic and adult spinal cord, where they maintain this ability to respond to external injury cues and factors [42], making them viable cellular targets for a variety of endogenous repair strategies.

Our findings examine the fundamental biology of brain NSCs and we show that pNSCs from the late prenatal brain give rise to bipotential neuron/astrocyte NPCs, some bipotential neuron/oligodendrocyte NPCs, and *GFAP*-expressing neuronally specified NPCs. We also show that specification, but not maturation, of the neuronal fate requires Nexn.

Our clonal retroviral lineage tracing suggests that NPCs specified to only make neurons, and to a lesser extent bipotent neuron/astrocyte NPCs, constitute the majority of continuously proliferating cells downstream of pNSCs in vitro. For dNSC-derived NPCs, proliferative astrocyte-only NPCs were found in roughly equal proportions to bipotent neuron/astrocyte NPCs, with bipotent NPCs from either NSC statistically being more proliferative than their unipotent counterparts.

Although we identified some overlapping and some distinct NPCs downstream of pNSCs and dNSCs, it is possible that more rare NPC types were missed, particularly downstream of pNSCs where fewer NPCs continue to proliferate by 7 days of clonal sphere growth. Further, no bipotent oligodendrocyte/neuronal NPCs were identified by clonal retroviral lineage tracing downstream of dNSCs, although these cells were seen downstream of pNSCs. No bipotential glial clones (astrocyte/oligodendrocyte) clones were seen downstream of either NSC type, as has been reported similarly by others for NPCs [21].

Performing the lineage tracing in vitro presents some limitations in terms of in vivo relevance; however, it does permit the study of the progenitors most immediately downstream of pNSCs, which is less feasible with in vivo studies given their rarity. The lineage relationships between pNSCs and dNSCs in vivo also presented a challenge: Although in the adult brain pNSC-derived progeny transplanted into the subependyma were shown to be able to migrate along the rostral migratory stream toward the olfactory bulb [2], it remained unclear whether pNSCs could directly generate NPCs or whether they must always pass through a dNSC intermediate.

More recent evidence using pNSC lineage tracing in vivo has demonstrated that pNSCs labeled in the late embryonic stages of brain development are able to make adult subependymal precursors [9] and our work herein shows different fate specification of neuronal progenitors downstream of pNSCs and dNSC, and thus a dNSC intermediate is not necessary to give rise to mature neural phenotypes.

Single-cell RNA-seq corroborated the in vitro lineage tracing findings of neuron/astrocyte bipotential progenitor cells. Of interest, we observed more cells of neuronal identity in the pNSC-derived scRNA-seq dataset even though neurons are not more numerous than astrocytes in differentiated pNSC-derived pNSC-derived neurospheres (Fig. 1A).

This may be due to a selective survival effect during the Drop-seq protocol; however, neuronally specified clones also were more frequent in the proliferation-dependent RV lineage tracing than astrocyte-specified clones. This is consistent with the idea that during neurosphere formation there are far more neuronally specified cells that do not later survive during differentiation, or that neuronal NPCs remain proliferating for longer than glial NPCs.

Our finding of a rare bipotential neuron/oligodendrocyte progenitor downstream of pNSCs in lineage tracing is supported by single-cell RNA-sequencing. *Dlx1 and Dlx2* have been reported to control neuronal versus oligodendrocyte fate in a common progenitor [43], and indeed we saw expression of both of these genes in cells that contain oligodendrocyte candidate marker myelin basic protein as well as cells in the neuronal clusters, providing further transcriptional evidence of a bipotent neuronal/oligodendrocyte progenitor cell.

We have previously reported that oligodendrocyte production by pNSCs peaks in the early postnatal period [8], so whether this bipotential progenitor exists in preparation for this period or persists into the adult brain remains to be explored.

Cluster 5 in the single-cell RNA sequencing data, the proliferative cells, showed an overlap in neuronal/astrocyte cell fate markers, suggesting that it may contain the bipotential neuron/astrocyte clones observed with clonal lineage tracing. In addition to corroborating each of the unipotent and bipotent NPC types, the single-cell transcriptomics data also suggested that there is significant lineage priming in NPCs derived from pNSCs, with substantial overlap of markers for unique mature neuronal cell types.

Indeed, it was a surprise to see mature markers such as MBP, Npy, Pvalb, and Aqp4 already expressed in undifferentiated precursors, and whether this reflects priming only at the transcriptional level has yet to be investigated. Similarly, neurotransmitter pathway markers for glutamate versus GABA neurons were found in the same single precursor cells, suggesting that pNSCs may retain some ability to make both cortical and subcortical neurons.

Trajectory analysis using p-Creode suggested the existence of an additional route for pNSCS to make olfactory bulb neurons, whereas other subtypes of neurons such as striatal and cortical interneurons had shared developmental pathways. This could be indicative of a bias to OB

interneuron production at E17. The trajectory analyses also revealed a central branching area that appeared to be the origin of most progenitor cell types. This region may be the origin of all pNSC lineages, and presumably would be where the rare pNSCs would potentially be found (Fig. 5, arrow)

The wide array of neuronal subtypes seen in cells from pNSC-derived neurospheres in the scRNA-seq analysis may indicate that pNSCs, as more rare and upstream NSCs, have more flexibility in terms of the neuronal subtypes they can make than dNSCs. Indeed, pNSCs appear to retain the potential to make neuronal subtypes beyond a very early developmental window. For example, many interneurons of the cortex already would have left the ventral germinal zone by E17.5 [44].

dNSCs, which are responsible for the majority of GABAergic neuron production during development and homeostasis in adulthood, may need to produce more striatal GABA neurons destined to form specific regional neuronal subtypes. Regionalization of neuronal-subtype specification has been reported for *GFAP*-expressing dNSCs [45–47].

Alternatively, since pNSCs are mostly quiescent in the adult brain and always rare in frequency [2,3], it is possible that pNSCs produce neuronal progenitors that are uncommitted to a specific subtype of neuron because they have not had selective phylogenetic pressure for more specific neuronal fate commitment. Indeed, given their ability to respond quickly to injury [2] and repopulate the ablated dNSC neural lineage [3], it is possible that pNSCs remain primed for multiple lineages, enabling more flexibility in regenerative potential.

Perhaps this overlap of expression of regional neuronal transcripts in pNSC-derived NPCs may reflect pNSCs being the earliest NSC during development (as they arise just after gastrulation [40,31,41,48]), and therefore they retain the ability to make multiple neuronal cell types. This expanded neuronal potential may have evaded selective ontogenetic pressures for lineage restriction due to their rarity and quiescence in the adult, or perhaps because there is a lack of selective pressure for brain patterning in the earliest embryo when pNSCs arise [49].

This inherent flexibility of pNSC-derived precursors may be advantageous for faster regeneration after injury or quickly responding to homeostatic imbalances during development. Notably, this flexibility may not be specific to pNSC-NPCs, as limited specification of neural progenitors at the mRNA level has been reported in striatal precursors [50].

Last, we characterized Nexn as a functional marker for specification of neuronal progenitors downstream of pNSCs. Indeed, we demonstrate that Nexn is required for neuronal specification, but not maturation since neurites could still form in the few neurons that were generated after Nexn knockdown. The finding that this specification happens while cells are still proliferating supports a priming model of lineage commitment in neuronal precursors derived from pNSCs.

We suggest that Nexn is necessary for the specification rather than the survival and maturation of neuronal precursors, since we did not observe a change in the number of cells in differentiated neurospheres after Nexn knockdown and the few neurons that were produced still could grow long neurite processes.

Herein, we find several lines of evidence that pNSC-derived precursors retain some flexibility in their lineage: (1) there are bipotential NPCs in the in vitro lineage tracing; (2) NPCs co-express neuronal and astrocyte markers according to scRNA-seq; and (3) specification of neuronal progenitors occurs before neuronal maturation. These data suggest that in the brain, the most upstream NSC, the pNSC, produces progeny with a less traditional lineage hierarchy, perhaps similar to models for hematopoietic stem cell lineages [51–54].

Instead of a stepwise progressive commitment of progenitors, the progenitors downstream of pNSCs retain the capacity to make multiple cell types, both between neural lineages and within the neuronal lineage. The expanded potential of pNSCs and their NPCs to be specified (including at the transcriptional level) to make multiple neuronal cell types is consistent with their eventual role in the adult brain as a reserve pool of normally quiescent brain stem cells.

Author Disclosure Statement

The authors declare no competing interests.

Funding Information

This paper was supported by CIHR Foundation Grant FDN-148407 to Derek van der Kooy and CIHR grant MOP-125876 to Cindi Morshead.

Single-cell RNA sequencing data generated in this study have been deposited to GEO, Accession number GSE20 6844.

Supplementary Material

Supplementary Figure S1
Supplementary Figure S2
Supplementary Figure S3

References

1. Seaberg RM and D van der Kooy. (2003). Stem and progenitor cells: the premature desertion of rigorous definitions. Trends Neurosci 26(3):125–131.
2. Sachewsky N, R Leeder, W Xu, KL Rose, F Yu, D van der Kooy, and CM Morshead. (2014). Primitive neural stem cells in the adult mammalian brain give rise to GFAP-expressing neural stem cells. Stem Cell Reports 2:810–824.
3. Reeve RL, SZ Yammine, CM Morshead, and D van der Kooy. (2017). Quiescent Oct4 neural stem cells (NSCs) repopulate ablated glial fibrillary acidic protein NSCs in the adult mouse brain. Stem Cells 35:2071–2082.
4. Morshead CM, BA Reynolds, CG Craig, MW McBurney, WA Staines, D Morassutti, S Weiss, and D van der Kooy. (1994). Neural stem cells in the adult mammalian forebrain: a relatively quiescent subpopulation of subependymal cells. Neuron 13:1071–1082.
5. Doetsch F, I Caillé, DA Lim, JM García-Verdugo, and A Alvarez-Buylla. (1999). Subventricular zone astrocytes are neural stem cells in the adult mammalian brain. Cell 97: 703–716.
6. Codega P, V Silva-Vargas, A Paul, AR Maldonado-Soto, AM Deleo, E Pastrana, and F Doetsch. (2014). Prospective identification and purification of quiescent adult neural stem cells from their in vivo niche. Neuron 82:545–559.

7. DeVeale B, D Bausch-Fluck, R Seaberg, S Runciman, V Akbarian, P Karpowicz, C Yoon, H Song, R Leeder, et al. (2014). Surfaceome profiling reveals regulators of neural stem cell function. Stem Cells 32:258–268.
8. Reeve RL, SZ Yammine, B DeVeale, and D van der Kooy. (2016). Targeted activation of primitive neural stem cells in the mouse brain. Eur J Neurosci 43:1474–1485.
9. Sachewsky N, W Xu, T Fuehrmann, D van der Kooy, and CM Morshead. (2019). Lineage tracing reveals the hierarchical relationship between neural stem cell populations in the mouse forebrain. Sci Reports 9:17730.
10. Krushel LA, JG Johnston, G Fishell, R Tibshirani, D and van der Kooy. (1993). Spatially localized neuronal cell lineages in the developing mammalian forebrain. Neuroscience 53:1035–1047.
11. Temple S. (1989). Division and differentiation of isolated CNS blast cells in microculture. Nature 340:471–473.
12. Walsh C and CL Cepko. (1992). Widespread dispersion of neuronal clones across functional regions of the cerebral cortex. Science 255:434–440.
13. Guo C, MJ Eckler, WL McKenna, GL McKinsey, JL Rubenstein, B Chen. (2013). Fezf2 expression identifies a multipotent progenitor for neocortical projection neurons, astrocytes, and oligodendrocytes. Neuron 80(5):1167–1174.
14. Luskin MB, AL Pearlman, and JR Sanes. (1988). Cell lineage in the cerebral cortex of the mouse studied in vivo and in vitro with a recombinant retrovirus. Neuron 1:635–647.
15. Magavi S, D Friedmann, G Banks, A Stolfi, and C Lois. (2012). Coincident generation of pyramidal neurons and protoplasmic astrocytes in neocortical columns. J Neurosci 32(14):4762–4772.
16. Price J and L Thurlow. (1988). Cell lineage in the rat cerebral cortex: a study using retroviral-mediated gene transfer. Development 104:473–482.
17. Temple S and MC Raff. (1985). Differentiation of a bipotential glial progenitor cell in single cell microculture. Nature 313:223.
18. Vaysse PJ and JE Goldman. (1990). A clonal analysis of glial lineages in neonatal forebrain development in vitro. Neuron 5(3):227–235.
19. Luskin MB, JG Parnavelas, and JA Barfield. (1993). Neurons, astrocytes, and oligodendrocytes of the rat cerebral cortex originate from separate progenitor cells: an ultrastructural analysis of clonally related cells. J Neurosci 13: 1730–1750.
20. Williams BP, J Read, and J Price. (1991). The generation of neurons and oligodendrocytes from a common precursor cell. Neuron 7(4):685–693.
21. Shen Z, Y Lin, J Yang, DJ Jörg, Y Peng, X Zhang, Y Xu, L Hernandez, J Ma, and BD Simons. (2021). Distinct progenitor behavior underlying neocortical gliogenesis related to tumorigenesis. Cell Reports 34(11):108853.
22. Bush TG, N Puvanachandra, CH Horner, A Polito, T Ostenfeld, CN Svendsen, L Mucke, MH Johnson, and MV Sofroniew. (1999). Leukocyte infiltration, neuronal degeneration, and neurite outgrowth after ablation of scar-forming, reactive astrocytes in adult transgenic mice. Neuron 23:297–308.
23. Chiasson BJ, V Tropepe, CM Morshead, and D van der Kooy. (1999). Adult mammalian forebrain ependymal and subependymal cells demonstrate proliferative potential, but only subependymal cells have neural stem cell characteristics. J Neurosci 19:4462–4471.
24. Coles-Takabe BLK, I Brain, KA Purpura, P Karpowicz, PW Zandstra, CM Morshead, and D van der Kooy. (2008). Don't look: growing clonal versus nonclonal neural stem cell colonies. Stem Cells 26:2938–2944.
25. Macosko EZ, A Basu, R Satija, J Nemesh, K Shekhar, M Goldman, I Tirosh, AR Bialas, N Kamitaki, et al. (2015). Highly parallel genome-wide expression profiling of individual cells using nanoliter droplets. Cell 161:1202–1214.
26. Lun ATL, K Bach, and JC Marioni. (2016). Pooling across cells to normalize single-cell RNA sequencing data with many zero counts. Genome Biol 17:75.
27. Lun ATL, DJ McCarthy, and JC Marioni. (2016). A step-by-step workflow for low-level analysis of single-cell RNA-seq data with Bioconductor. F1000Res 5:2122.
28. Innes BT, Bader GD. (2018). scClustViz – Single-cell RNAseq cluster assessment and visualization. ISCB CommJ-1522.
29. Yuzwa SA*, MJ Borrett, BT Innes, A Voronova, T Ketela, DR Kaplan, GD Bader, and FD Miller. (2017). Developmental emergence of adult neural stem cells as revealed by single cell transcriptional profiling. Cell Reports 21:3970–3986.
30. Longair MH, DA Baker DA, and JD Armstrong. (2011). Simple Neurite Tracer: Open Source software for reconstruction, visualization and analysis of neuronal processes. Bioinformatics 27(17):2453–2454.
31. Hitoshi S, RM Seaberg, C Koscik, T Alexson, S Kusunoki, I Kanazawa, S Tsuji, and D van der Kooy. (2004). Primitive neural stem cells from the mammalian epiblast differentiate to definitive neural stem cells under the control of Notch signaling. Genes Dev 18:1806–1811.
32. Bayer SA, J Altman, XF Dai, and L Humphreys. (1991). Planar differences in nuclear area and orientation in the subventricular and intermediate zones of the rat embryonic neocortex. J Comp Neurol 307(3):487–498.
33. Bayraktar OA, LC Fuentealba, A Alvarez-Buylla, and DH Rowitch. (2014). Astrocyte development and heterogeneity. Cold Spring Harbour Perspect Biol 7(1):a020362.
34. Kohwi M and CQ Doe. (2013). Temporal fate specification and neural progenitor competence during development. Nat Rev Neurosci 14:823.
35. Garcia AD, NB Doan, T Imura, TG Bush, and MV Sofroniew. (2004). GFAP-expressing progenitors are the principal source of constitutive neurogenesis in adult mouse forebrain. Nat Neurosci 7:1233–1241.
36. Allen JP, GJ Hathway, NJ Clarke, MI Jowett, S Topps, KM Kendrick, PPA Humphrey, LS Wilkinson, and PC Emson. (2003). Somatostatin receptor 2 knockout/lacZ knockin mice show impaired motor coordination and reveal sites of somatostatin action within the striatum. Eur J Neurosci 17(9):1881–1895.
37. Liu LYM, MH Lin, JP Jiang, YC Huang, LE Jao, and YJ Chuang. (2016). Motor neuron-derived Thsd7a is essential for zebrafish vascular development via the Notch-dll4 signaling pathway. J Biomed Sci 23(1):59.
38. Herring CA, A Banerjee, ET McKinley, AJ Simmons, J Ping, JT Roland, JL Franklin, Q Liu, MJ Gerdes, RJ Coffey, and KS Lau. (2018). Unsupervised trajectory analysis of single-cell RNA-Seq and imaging data reveals alternative tuft cell origins in the gut. Cell Syst 6:37–51.e39.
39. Zhu B, C Rippe, J Holmberg, S Zeng, L Perisic, S Albinsson, U Hedin, B Uvelius, and K Swärd. (2018). Nexilin/NEXN controls actin polymerization in smooth

muscle and is regulated by myocardin family coactivators and YAP. Sci Reports 8(1):13025.
40. Tropepe V, S Hitoshi, C Sirard, TW Mak, J Rossant, and D van der Kooy. (2001). Direct neural fate specification from embryonic stem cells: a primitive mammalian neural stem cell stage acquired through a default mechanism. Neuron 30:65–78.
41. Smukler SR, SB Runciman, S Xu, and D van der Kooy. (2006). Embryonic stem cells assume a primitive neural stem cell fate in the absence of extrinsic influences. J Cell Biol 172:79–90.
42. Xu W, N Sachewsky, A Azimi, M Hung, A Gappasov, and CM Morshead. (2017). Myelin basic protein regulates primitive and definitive neural stem cell proliferation from the adult spinal cord. Stem Cells 35:485–496.
43. Petryniak MA, GB Potter, DH Rowitch, and JLR Rubenstein. (2007). Dlx1 and Dlx2 control neuronal versus oligodendroglial cell fate acquisition in the developing forebrain. Neuron 55(3):417–433.
44. Anderson SA, DD Eisenstat, L Shi, and JL Rubenstein. (1997). Interneuron migration from basal forebrain to neocortex: dependence on Dlx genes. Science 278:474–476.
45. Hitoshi S, V Tropepe, M Ekker, and D van der Kooy. (2002). Neural stem cell lineages are regionally specified, but not committed, within distinct compartments of the developing brain. Development 129:233–244.
46. Merkle FT, LC Fuentealba, TA Sanders, L Magno, N Kessaris, A Alvarez-Buylla. (2014). Adult neural stem cells in distinct microdomains generate previously unknown interneuron types. Nat Neurosci 17(2):207–214.
47. Fuentealba LC, SB Rompani, JI Parraguez, K Obernier, R Romero, CL Cepko, A Alvarez-Buylla. (2015). Embryonic origin of postnatal neural stem cells. Cell 161(7):1644–1655.
48. Chaddah R, M Arntfield, S Runciman, L Clarke, and D van der Kooy. (2012). Clonal neural stem cells from human embryonic stem cell colonies. J Neurosci 32:7771–7781.
49. Bizzotto S, Y Dou, J Ganz, RN Doan, M Kwon, CL Bohrson, SN Kim, T Bae, A Abyzov, NIMH Brain Somatic Mosaicism Network, PJ Park, and CA Walsh. (2021). Landmarks of human embryonic development inscribed in somatic mutations. Science 371:1249–1253.
50. Mayer C, C Hafemeister, RC Bandler, R Machold, R Batista Brito, X Jaglin, K Allaway, A Butler, G Fishell, and R Satija. (2018). Developmental diversification of cortical inhibitory interneurons. Nature 555:457–462.
51. Velten L, Haas SF, Raffel S, Blaszkiewicz S, Islam S, Hennig BP, Hirche C, Lutz C, Buss EC, et al. (2017). Human haematopoietic stem cell lineage commitment is a continuous process. Nat Cell Biol 19:271–281.
52. Rodriguez-Fraticelli AE, Wolock SL, Weinreb CS, Panero R, Patel SH, Jankovic M, Sun J, Calogero RA, Klein AM, and Camargo FD. (2018). Clonal analysis of lineage fate in native haematopoiesis. Nature 553:212–216.
53. Yamamoto R, AC Wilkinson, J Ooehara, X Lan, CY Lai, Y Nakauchi, JK Pritchard, and H Nakauchi. (2018). Large-scale clonal analysis resolves aging of the mouse hematopoietic stem cell compartment. Cell Stem Cell 22(4): 600–607.
54. Pei W, TB Feyerabend, J Rössler, X Wang, D Postrach, K Busch, I Rode, K Klapproth, N Dietlein, et al. (2017). Polylox barcoding reveals haematopoietic stem cell fates realized in vivo. Nature 548(7668):456–460.

Address correspondence to:
Derek van der Kooy, PhD
Department of Molecular Genetics
University of Toronto
160 College Street, CCBR, Room 1102
Toronto ON, M5S 3E1
Canada

E-mail: derek.van.der.kooy@utoronto.ca

Received for publication February 19, 2023
Accepted after revision August 3, 2023
Prepublished on Liebert Instant Online August 8, 2023